

# Synthesis of Mn<sub>3</sub>O<sub>4</sub> Microflowers Anode Material for Lithium-ion Batteries with Enhanced Performance

## ABSTRACT

It is important to prepare novel micro-nanostructures of Mn oxides for energy storage. A simple and versatile method for preparation of Mn<sub>3</sub>O<sub>4</sub> microflowers associated with super-thin nanosheets is developed via a solvo-thermal approach, which are tested as a new high-capacity anode material for lithium-ion batteries. It shows better cycling performance than Mn<sub>3</sub>O<sub>4</sub> nanoparticles. Research on this topic mainly sheds some light on the preparation of three-dimensional flower-like oxide hierarchical architectures with improved electrochemical performance for energy storage.

*Keywords: Manganese oxide; Hierarchical architectures; Anode; Lithium-ion battery; Surfactant; Nanosheet.*

## 1. INTRODUCTION

Rechargeable batteries with reversible and efficient electrochemical energy storage and conversion are urgent in various applications, such as portable electronic consumer devices, electric vehicles, and large-scale electricity storage in smart and intelligent grids as renewable and clean energy[1, 2]. Lithium-ion battery is one of the fascinating rechargeable batteries for high energy density coupled with a long life cycle and charge-discharge rate capability[3]. Studies have been conducted to develop low-cost, sustainable, renewable, safe, and high-energy density electrode materials for lithium-ion batteries. Considering environmental safety, researchers should prepare potential electrode materials for lithium-ion batteries through green chemistry based on simple and inexpensive procedures.

Manganese based anode materials are less toxic, abundant in natural resources[4]. Though Mn<sub>3</sub>O<sub>4</sub> is isostructural with Co<sub>3</sub>O<sub>4</sub>, it has poor lithiation activity and electrically insulating, resulting in fast capacity decay as anode materials for lithium-ion batteries. Recently great progress has been achieved for Mn<sub>3</sub>O<sub>4</sub> anode materials. The improved electrochemical properties turned true via the following methods. Mesoporous carbon, graphene, carbon nanotube and various carbon nanostructures were introduced to prepare carbon based Mn<sub>3</sub>O<sub>4</sub> nano-composites. These composites showed better cycling stability and higher discharge capacity than bulk Mn<sub>3</sub>O<sub>4</sub> for fast ion diffusion, good electronic conductivity, and skeleton supporting function[5-35]. People also designed various Mn<sub>3</sub>O<sub>4</sub> nanostructures to improve the cycling performance of Mn<sub>3</sub>O<sub>4</sub>. In these Mn<sub>3</sub>O<sub>4</sub> nanostructures, well-shaped nanostructure, pore, hollow structure and 3D array played an important role in the long cycling performance. Novel pongelike nanosized Mn<sub>3</sub>O<sub>4</sub> exhibits a high initial reversible capacity of 869 mA h g<sup>-1</sup> and significantly enhanced first coulomb efficiency with a stabilized reversible capacity of around 800 mA h g<sup>-1</sup> after over 40 charge/discharge cycles [4]. Mn<sub>3</sub>O<sub>4</sub> hollow microspheres demonstrate a good electrochemical performance, with a high reversible capacity of 646.9 mA h g<sup>-1</sup> after 240 cycles at a current density of 200 mA h g<sup>-1</sup>[36]. While fluorinated Mn<sub>3</sub>O<sub>4</sub> nanospheres for lithium-ion batteries show poor cycling performances[37]. 3D porous Mn<sub>3</sub>O<sub>4</sub> nanosheet arrays could be directly used as a binder-free and conductive-agent-free electrode to deliver ultrahigh electrochemical performance [38]. It is reported that the 3D pores and voids between the nanosheet arrays could provide rapid ion transfer channels, as well as accommodating the volumetric changes of Mn<sub>3</sub>O<sub>4</sub> during the electrochemical cycling[38]. The ultrathin Mn<sub>3</sub>O<sub>4</sub> nanosheets exhibit a high reversible capacity and stronger cycling stability for high surface area[39]. The well-shaped Mn<sub>3</sub>O<sub>4</sub> tetragonal bipyramids with high-energy facets show a high initial discharge capacity. In addition, the anode displays a good fast rate performance and delivers a reversible capacity of 822.3 mA h g<sup>-1</sup> (the theoretical capacity: 937 mA h g<sup>-1</sup> at a current density of 0.2 C after 50 cycles[40]. The porous Mn<sub>3</sub>O<sub>4</sub> nanorods can improve electrochemical reaction kinetics and favor the formation of Mn<sub>3</sub>O<sub>4</sub> [41]. Mn<sub>3</sub>O<sub>4</sub> nano-octahedra has a discharge capacity of 667.9 mA h g<sup>-1</sup> after 1000 cycles at 1.0 A g<sup>-1</sup> ascribed to the lower charge transfer resistance due to the exposed highly active {011} facets, which can facilitate the conversion reaction of Mn<sub>3</sub>O<sub>4</sub> and Li owing to the alternating Mn and O atom layers,

49 resulting in easy formation and decomposition of the amorphous  $\text{Li}_2\text{O}$  and the multi-electron  
50 reaction[42]. The hollow  $\text{Mn}_3\text{O}_4$  spheres deliver a highly stable cycle performance with capacity  
51 retention of similar to  $980 \text{ mA h g}^{-1}$  for over 140 cycles at  $200 \text{ mA g}^{-1}$  and an excellent rate  
52 capability[43]. It can be seen that  $\text{Mn}_3\text{O}_4$  with nanosheets, pore, high surface area and interconnected  
53 voids are apt to show high discharge capacity and long cycling stability. The 3D assembling  $\text{Mn}_3\text{O}_4$   
54 microflowers assembling with nanosheets are expected to show favorable electrochemical  
55 performances for the presence of voids among the nanosheet arrays. There are few reports on the  
56 research of  $\text{Mn}_3\text{O}_4$  microflowers except  $\text{Mn}_3\text{O}_4\text{-Fe}_3\text{O}_4$  and  $\text{MnO- Mn}_3\text{O}_4$  nanoflowers.  $\text{Mn}_3\text{O}_4\text{-Fe}_3\text{O}_4$   
57 nanoflowers are simply fabricated through one step etching  $\text{Mn}_5\text{Fe}_5\text{Al}_{90}$  ternary alloy, which exhibits  
58 higher performance as anode material for lithium ion batteries than that of pure  $\text{Mn}_3\text{O}_4$  and  $\text{Mn}_3\text{O}_4$   
59 anodes for unique hierarchical flower-like structure and the synergistic effects between  $\text{Mn}_3\text{O}_4$  and  
60  $\text{Mn}_3\text{O}_4$  [44]. A hierarchically porous  $\text{MnO- Mn}_3\text{O}_4$  nano-flowers can be fabricated by dealloying  $\text{Mn/Al}$   
61 alloys in aqueous  $\text{NaOH}$  solution in the presence of  $\text{H}_2\text{O}_2$ , and upon annealing, which has a capacity  
62 of 1018, 901 and  $757 \text{ mA h g}^{-1}$  with nearly 100% retention capacity after 100, 200 and  
63  $500 \text{ mA g}^{-1}$ [45].  $\text{Mn}_3\text{O}_4$  nanosheets associated with nanorods can be assembled to 3D flower-like  
64  $\text{Mn}_3\text{O}_4$  with hexadecyl trimethyl ammonium bromide (CTABr), urea and  $\text{MnSO}_4$  as reagents, while  
65 they did not tested any properties, e.g. batteries [46].

66 In this study, a simple method was developed to prepare  $\text{Mn}_3\text{O}_4$  microflowers associated with  
67 nanosheets. These microflowers were synthesized in a  $\text{N,N}$ -dimethylformamide (DMF)–water solution  
68 with the aid of CTABr. When tested as an anode material for lithium-ion batteries, the  $\text{Mn}_3\text{O}_4$   
69 microflowers exhibited enhanced cycling stability than  $\text{Mn}_3\text{O}_4$  nanoparticles.

70

## 71 **2. MATERIAL AND METHODS / EXPERIMENTAL DETAILS / METHODOLOGY (ARIAL,** 72 **BOLD, 11 FONT, LEFT ALIGNED, CAPS)**

73

74 All chemicals are commercially available. The preparation was performed via a solvothermal method  
75 in a DMF-water mixed solvent. In a typical procedure, 1 mmol manganese acetate tetrahydrate and  
76 0.5 g hexadecyl trimethyl ammonium bromide (CTABr) were added to a 5 ml DMF- 25 ml water  
77 solution and stirred at room temperature for 2 hours. After that, the mixture was transferred to a 50-ml  
78 Teflon-lined stainless autoclave, sealed, kept at  $200 \text{ }^\circ\text{C}$  for 24 hours, cooled to room temperature,  
79 washed with absolute alcohol and dried at  $70 \text{ }^\circ\text{C}$  for 12 hours (marked with DT-1). Sample DT-2 was  
80 prepared without CTABr under the identical condition. While Sample DT-3 was prepared with 30 ml  
81 water in the absence of CTABr.

82 The morphological characteristics of the as-synthesized materials were observed with a Hitachi S-  
83 4800 field emission scanning electron microscope (SEM). X-ray diffraction (XRD) patterns were  
84 recorded on a diffract meter (Co  $\text{K}\alpha$ , Analytical, and Pert). Cyclic voltammetry (CV) experiments were  
85 performed with a Chi660c electrochemical workstation at a scan rate of  $1 \text{ mV S}^{-1}$ . A Land CT2001A  
86 battery tester was used to measure the electrode activities at room temperature.

87 The as-synthesized samples were tested as anode materials for lithium-ion batteries. The composite  
88 of negative electrode material was consisted of the active material, a conductive material (super-pure  
89 carbon) and binder polyvinylidene difluoride (PVDF) in a weight ratio of 7/2/1. The Li metal was used  
90 as the counter electrode. The cells were charged and discharged between a 0.05 - 3.0 V voltage limit.

91

## 92 **3. RESULTS AND DISCUSSION**

93

94 Three samples were obtained by adjusting synthesis parameters. Both DMF and CTABr play an  
95 important role in the formation of different morphologies. When water was used as the solvent in the  
96 absence of CTABr, the sample appears as monodispersed nanoparticles between 30 and 150 nm in  
97 Fig. 1a,b. While DMF was added, thin microplatelets were obtained, as shown in Fig. 1c, d. The  
98 length and width of microplatelets can be up to several  $\mu\text{m}$ . There are also some thin nanobelts.  
99 Some microflowers composed of superimposed thin and wide nanosheets were prepared with CTABr  
100 in the DMF- $\text{H}_2\text{O}$  mixed solvent in Fig. 1e, f. Certain microflower is several  $\mu\text{m}$  in size.

101

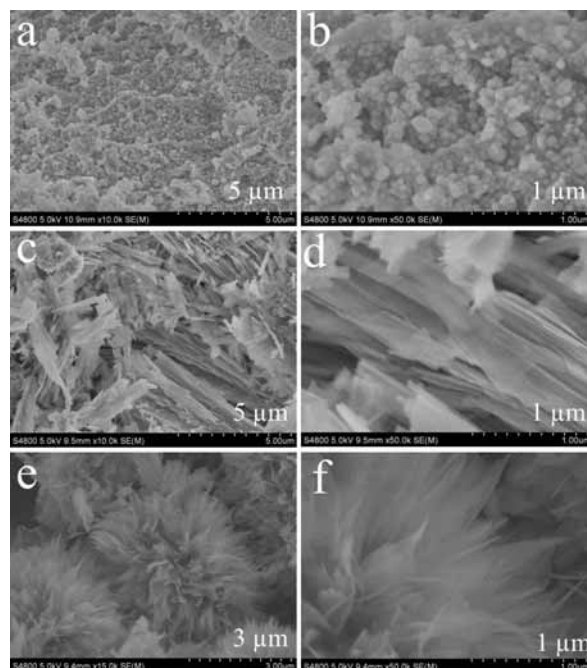
102 X-ray diffraction was performed to identify the structure of the three samples. It can be seen that  
103 CTABr plays an important role in the crystallization of products. The diffraction peaks of the sample  
104 prepared with DMF, water and CTABr has the highest intensity than samples prepared with water,

105 CTABr and DMF in Fig. 2. The diffraction peaks can be ascribed to  $\text{Mn}_3\text{O}_4$  in Fig. 2a (JCPDS 89-  
106 4837). The other samples can also be ascribed to  $\text{Mn}_3\text{O}_4$  in Fig. 2b,c, respectively. All the  $\text{Mn}_3\text{O}_4$   
107 here are lack of the peak of (101), which means that the is not the high-energy {101} plane.

108  
109 The electrochemical performance of  $\text{Mn}_3\text{O}_4$  nanoparticles and microflowers was evaluated as anode  
110 materials for lithium-ion batteries (Fig. 3). Fig. 3a shows the 1<sup>st</sup> and 2<sup>nd</sup> charge–discharge profiles of  
111  $\text{Mn}_3\text{O}_4$  microflowers at a current density of 240  $\text{mA g}^{-1}$  (Sample T-72). A long discharge platform is  
112 observed at 0.5 V in the first discharge curve, but this platform disappears in the succeeding  
113 discharge curves. The  $\text{Mn}_3\text{O}_4$  microflowers-based composite electrode delivers an initial discharge  
114 capacity of 1496  $\text{mA h g}^{-1}$ . However, the 1<sup>st</sup> discharge profiles of  $\text{Mn}_3\text{O}_4$  nanoparticles show four  
115 discharge platforms at 0.33, 0.44, 0.92 and 1.3 V, implying that a multi-step conversion reaction takes  
116 place. A new platform at 0.7 V appears in the succeeding discharge curves. The  $\text{Mn}_3\text{O}_4$   
117 nanoparticles-based composite electrode delivers an initial discharge capacity of 1280  $\text{mA h g}^{-1}$ . It  
118 can be seen that  $\text{Mn}_3\text{O}_4$  without high-energy {101} plane can also have a very high initial discharge  
119 capacity. It can also be found that  $\text{Mn}_3\text{O}_4$  nanoparticles have a steeper charge curve than  $\text{Mn}_3\text{O}_4$   
120 microflowers between 1.4 and 3.0 V implying that a severe polarization takes place in the  $\text{Mn}_3\text{O}_4$   
121 nanoparticles-based composite electrode.

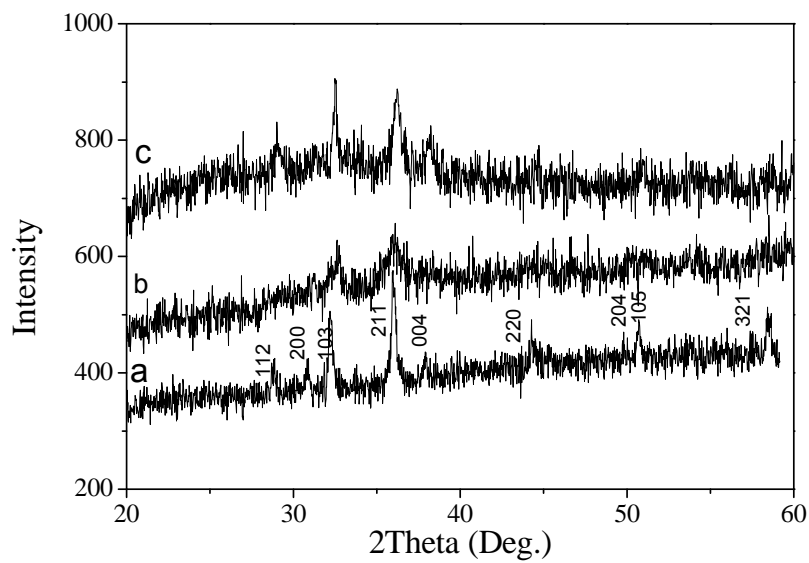
122  
123 We also performed the  $dQ/dV \sim V$  curves obtained from the 1<sup>st</sup> and 2<sup>nd</sup> charge-discharge curves of  
124  $\text{Mn}_3\text{O}_4$  nanoparticles and microflowers in Fig. 4. In the first charge-discharge cycle of  $\text{Mn}_3\text{O}_4$   
125 nanoparticles, four reduction peaks are centered at 0.33, 0.45, 0.90 and 1.3 V, and the oxidation peak  
126 is at 1.24 V in Fig. 4a. In the first charge-discharge cycle of  $\text{Mn}_3\text{O}_4$  microflowers, the reduction and  
127 oxidation peaks are centered at 0.33 and 1.28 V in Fig. 4b, respectively. In the second charge-  
128 discharge cycle of  $\text{Mn}_3\text{O}_4$  nanoparticles, two reduction peaks are centered at 0.45 and 0.52 V, and the  
129 oxidation peak is at 1.24 V in Fig. 5b. In the second charge-discharge cycle of  $\text{Mn}_3\text{O}_4$  microflowers,  
130 the reduction and oxidation peaks are centered at 0.54 and 1.25 V in Fig. 2, respectively. The  
131 reduction peaks in the range of 1.3–0.4 V was ascribed to reduction from Mn(III) to Mn(II), and the 0.4–  
132 0.1 V range reflected the reduction from Mn(II) to Mn(0) [47,48]. The difference of first discharge curve  
133 between  $\text{Mn}_3\text{O}_4$  microflowers and nanoparticles is because  $\text{Mn}_3\text{O}_4$  microflowers only undergoes the  
134 reduction from Mn(II) to Mn(0). While  $\text{Mn}_3\text{O}_4$  nanoparticles undergo reductions from Mn(III) to Mn(II) to  
135 Mn(0). In the second discharge process, In the second discharge, the contribution to discharge  
136 capacity is mainly ascribed to the reduction around 0.5 V. The  $\text{Li}^+$  charge reaction: is  $\text{Mn}_3\text{O}_4 + 8\text{Li}^+ +$   
137  $8\text{e}^-$  to  $3\text{Mn(0)} + 8\text{Li}_2\text{O}$  [49]. Compared to  $\text{Mn}_3\text{O}_4$  nanoparticles,  $\text{Mn}_3\text{O}_4$  microflowers does not undergo  
138 reduction from Mn(III) to Mn(II) and reduce polarization.

139  
140 Fig.6 is the cycling performance testes at current densities of 240 and 480  $\text{mA g}^{-1}$ . The  $\text{Mn}_3\text{O}_4$   
141 microflowers-based composite electrode delivers a second discharge capacity of 870.2 and 714.8  
142  $\text{mA h g}^{-1}$  in Fig. 6a,b, respectively. A reversible capacity of 392.8 and 358.5  $\text{mA h g}^{-1}$  is retained after  
143 20 cycles. The  $\text{Mn}_3\text{O}_4$  nanoparticles-based composite electrode show lower discharge capacity and  
144 worse cycling stability at current densities of 240 and 480  $\text{mA g}^{-1}$  in Fig. 6c,d. It delivers a second  
145 discharge capacity of 332.8 and 156.5  $\text{mA h g}^{-1}$ , respectively. The final discharge capacity is even low  
146 to 131.3 and 53.8  $\text{mA h g}^{-1}$ . The fast capacity decay of  $\text{Mn}_3\text{O}_4$  nanoparticles is due to the reduction  
147 from Mn(III) to Mn(II). The improved electrochemical performance of  $\text{Mn}_3\text{O}_4$  microflowers is due to  
148 reduce the activity of  $\text{Mn}_3\text{O}_4$ , avoid the complicated reduction from Mn(III) to Mn(II) and reduce  
149 polarization. We have focused on the research of flower-like rutile  $\text{TiO}_2$  and ammonium vanadium  
150 bronze. We found that the effect of flower-like nanostructures on the reaction kinetics of the electrode  
151 are ascribe to the changes the total impedance and electron transfer resistance [50, 51]. The improved  
152 performance of  $\text{Mn}_3\text{O}_4$  micro-flowers is also ascribed to improve the transferring of electron.



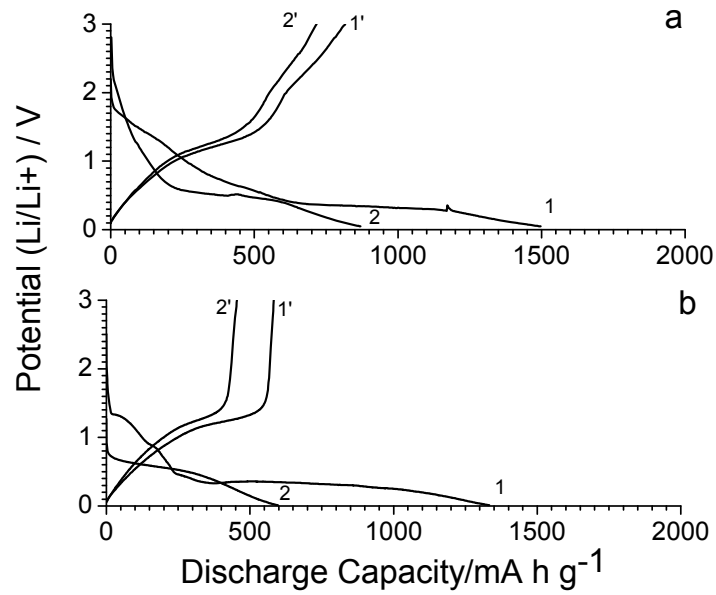
153  
154  
155  
156

**Fig. 1. SEM images of samples with (a, b) water, (c, d) water and DMF, and (e, f) water, DMF and CTABr**



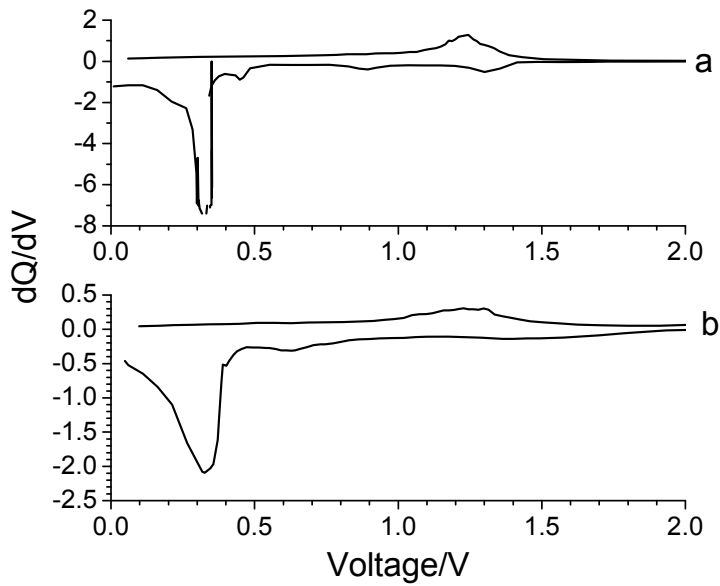
157  
158  
159  
160

**Fig. 2. Wide angle XRD patterns of samples with (a) water, DMF and CTABr, (b) water and DMF, and (c) water**



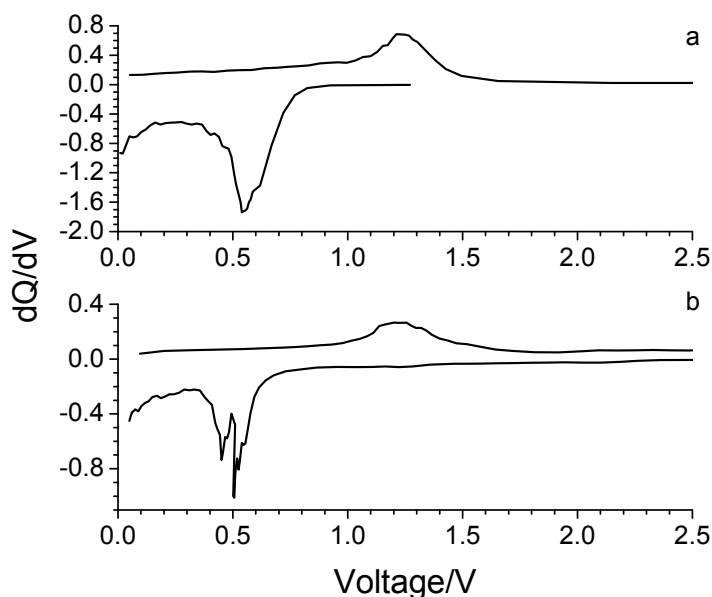
161  
162  
163  
164  
165

Fig. 3. The first and second charge–discharge profiles at a current density of 240 mA g<sup>-1</sup> of (a) Mn<sub>3</sub>O<sub>4</sub> microflowers and (b) Mn<sub>3</sub>O<sub>4</sub> nanoparticles



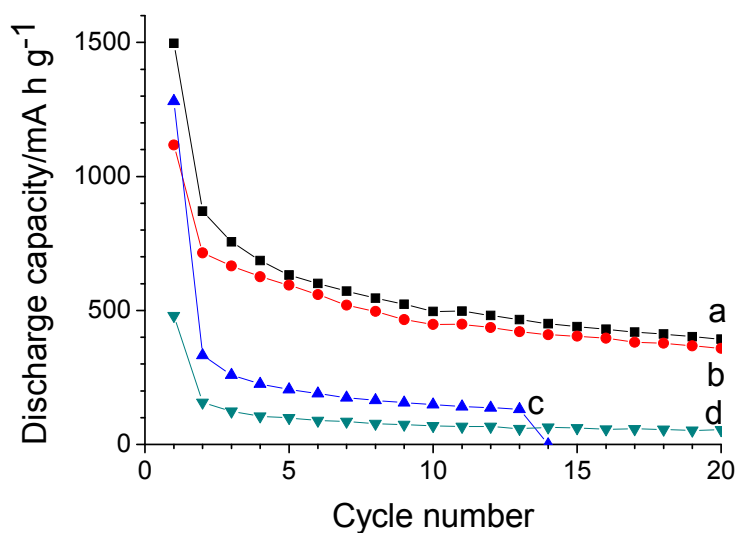
166  
167  
168  
169

Fig. 4. The dQ/dV-curve derived the first charge–discharge profiles of (a) Mn<sub>3</sub>O<sub>4</sub> nanoparticles (b) Mn<sub>3</sub>O<sub>4</sub>microflowers



170  
171  
172  
173  
174

Fig. 5. The  $dQ/dV$ -curve derived the second charge–discharge profiles of (a)  $Mn_3O_4$  microflowers (b)  $Mn_3O_4$  nanoparticles



175  
176  
177  
178  
179  
180  
181

Fig. 6. The cyclic performance tested at current densities of 240 and 480  $mA g^{-1}$  of (a, b)  $Mn_3O_4$  microflowers, and (c, d)  $Mn_3O_4$  nanoparticles

#### 4. CONCLUSION

182 In summary,  $Mn_3O_4$  microflowers associated with super-thin nanosheets were prepared by using a  
183 solvo-thermal method with the aid of surfactant CTABr. The  $Mn_3O_4$  microflowers exhibit better cycling  
184 stability and higher discharge capacity than  $Mn_3O_4$  nanoparticles as anode materials for lithium-ion  
185 batteries due to reduce the activity of  $Mn_3O_4$ , avoid the complicated reduction from Mn(III) to Mn(II)  
186 and reduce polarization. This simple method may also be used to fabricate other anode materials for  
187 lithium-ion batteries with improved electrochemical performance.

188  
189  
190  
191  
192  
193  
194  
195  
196  
197  
198  
199  
200  
201  
202  
203  
204  
205  
206  
207  
208  
209  
210  
211  
212  
213  
214  
215  
216  
217  
218  
219  
220  
221  
222  
223  
224  
225  
226  
227  
228  
229  
230  
231  
232  
233  
234  
235  
236  
237  
238  
239  
240  
241  
242  
243  
244  
245

## REFERENCES

1. Cheng FY, Liang J, Tao ZL, Chen J. Functional materials for rechargeable batteries. *Adv Mater.* 2012;23:1695-1715.
2. Fei HL, Liu X, Li ZW. Hollow cobalt coordination polymer microspheres: a promising anode material for lithium-ion batteries with high performance. *Chem Eng J.* 2015;281:453-458.
3. Tarascon JM. Key challenges in future Li-battery research. *Phil. Trans. R. Soc. A.*, 2010;368:3227-3241.
4. Gao J, Lowe MA, Abruña HD, Spongelike nanosized  $Mn_3O_4$  as a high-capacity anode material for rechargeable lithium batteries. *Chem Mater.* 2011;23:3223-3227.
5. Zhang LP, Li GS, Fan JM, Li BY. In situ synthesis of  $Mn_3O_4$  nanoparticles on hollow carbon nanofiber as high-performance lithium ion battery anode. *Chem.* 2018;DOI:10.1002/chem.201801196.
6. Guo LG, Ding Y, Qin CQ et al, Anchoring  $Mn_3O_4$  nanoparticles onto nitrogen-doped porous carbon spheres derived from carboxymethyl chitosan as superior anodes for lithium-ion batteries. *J Alloy Cmpd.* 2018;735:209-217.
7. Song NJ, Ma CL. A green synthesis of  $Mn_3O_4$  /graphene nanocomposite as anode material for lithium-ion batteries. *Int J Electrochem Sci.* 2018;13:452-460.
8. Wu LL, Zhao DL, Cheng XW, Ding ZW, Hu T, Meng S. Nanorod  $Mn_3O_4$  anchored on graphene nanosheet as anode of lithium ion batteries with enhanced reversible capacity and cyclic performance. *J Alloy Cmpd.* 2018;728:383-390.
9. Li Z, Tang B,  $Mn_3O_4$ /nitrogen-doped porous carbon fiber hybrids involving multiple covalent interactions and open voids as flexible anodes for lithium-ion batteries. *Green Chem.* 2017;19:5862-5873.
10. Liu BB, Qi L, Ye JJ, Wang JQ, Xu CX. Facile fabrication of graphene-encapsulated  $Mn_3O_4$  octahedra cross-linked with a silver network as a high-capacity anode material for lithium ion batteries, *New J Chem.* 2017;41:13454-13461.
11. Peng HJ, Hao GX, Chu ZH, Lin J, Lin XM, Cai YP. Mesoporous  $Mn_3O_4$ /C microspheres fabricated from MOF template as advanced lithium-ion battery anode. *Crys Growth & Des.* 2017;11:5881-5886.
12. Lv KK, Zhang YH, Zhang DY, Ren WW, Sun L.  $Mn_3O_4$  nanoparticles embedded in 3D reduced graphene oxide network as anode for high-performance lithium ion batteries. *J Mater Sci-Mater. El.*, 2017;28:14919-14927.
13. Pramanik A, Maiti S, Sreemany M, Mahanty S. Rock-salt-templated  $Mn_3O_4$  nanoparticles encapsulated in a mesoporous 2D carbon matrix: a high rate 2 V anode for lithium-ion batteries with extraordinary cycling stability. *Chemistryselect*, 2017;2:854-7864.
14. Zhang R, Wang D, Qin LC,  $MnCO_3$ / $Mn_3O_4$ /reduced graphene oxide ternary anode materials for lithium-ion batteries: facile green synthesis and enhanced electrochemical performance. *J Mater Chem A*, 2017;5:17001-17011.
15. Zhuang YC, Ma Z, Deng YM, Song XN, Zuo XX, Xiao X, Nan JM. Sandwich-like  $Mn_3O_4$ /carbon nanofragment composites with a higher capacity than commercial graphite and hierarchical voltage plateaus for lithium ion batteries. *Electrochim Acta.* 2017;440-447.
16. Yang ZL, Lu DL, Zhao RR, Gao AM, Chen HY. Synthesis of a novel structured  $Mn_3O_4$ @C composite and its performance as anode for lithium ion battery. *Mater Lett.* 2017;198:97-100.
17. Cui X, Wang YQ, Xu QY, Sun P, Wang XZ, Wei T, Sun YM. Carbon nanotube entangled  $Mn_3O_4$  octahedron as anode materials for lithium-ion batteries. *Nanotech.* 2017;28:255402.
18. Chen JY, Wu XF, Gong Y, Wang PF, Li WH, Tan QQ, Chen YF. Synthesis of  $Mn_3O_4$ /N-doped graphene hybrid and its improved electrochemical performance for lithium-ion batteries. *Ceram Int.* 2017;43:4655-4662.
19. Gangaraju D, Sridhar V, Lee I, Park H. Graphene - carbon nanotube -  $Mn_3O_4$  mesoporous nanoalloys as high capacity anodes for lithium-ion batteries. *J Alloy Cmpd.* 2017;699:106-111.
20. Seong CY, Park SK, Bae Y, Yoo S, Piao Y. An acid-treated reduced graphene oxide/  $Mn_3O_4$  nanorod nanocomposite as an enhanced anode material for lithium ion batteries. *Rsc Adv.* 2017;7:37502-37507.
21. Park I, Kim T, Park H, Mun M, Shim SE, Baek SH. Preparation and electrochemical properties of Pt-Ru/  $Mn_3O_4$ /C bifunctional catalysts for lithium-air secondary battery. *J Nanosci. Nanotechnol.* 2016;16:10453-10458.

- 246 22. Zhang Y, Yue KQ, Zhao HS, Wu Y, Duan LF, Wang KL. Bovine serum albumin assisted synthesis  
247 of Fe<sub>3</sub>O<sub>4</sub>@C@Mn<sub>3</sub>O<sub>4</sub> multilayer core-shell porous spheres as anodes for lithium ion battery.  
248 Chem Eng J. 2016;291:238-243.
- 249 23. Park SK, Seong CY, Yoo S, Piao Y. Porous Mn<sub>3</sub>O<sub>4</sub> nanorod/reduced graphene oxide hybrid paper  
250 as a flexible and binder-free anode material for lithium ion battery. Energy, 2016;99:266-273.
- 251 24. Alfaruqi MH, Gim J, Kim S, Song J, Duong PT, Jo J, Baboo JP, Xiu Z, Mathew V, Kim J. One-step  
252 pyro-synthesis of a nanostructured Mn<sub>3</sub>O<sub>4</sub>/C electrode with long cycle stability for rechargeable  
253 lithium-ion batteries. Chem-A Eur J. 2016; 22:2039-2045.
- 254 25. Bhimanapati G, Yang RG, Robinson JA, Wang Q. Effect of Mn<sub>3</sub>O<sub>4</sub> nanoparticle composition and  
255 distribution on graphene as a potential hybrid anode material for lithium-ion batteries. Rsc Adv.  
256 2016;6:33022-33030.
- 257 26. Jing MJ, Wang JF, Hou HS, Yang YC, Zhang Y, Pan CC, Chen J, Zhu YR, Ji XB. Carbon  
258 quantum dot coated Mn<sub>3</sub>O<sub>4</sub> with enhanced performances for lithium-ion batteries. J Mater Chem A.  
259 2015;3:16824-16830.
- 260 27. Ren YR, Wang JW, Huang XB, Yang B, Ding JN. One step hydrothermal synthesis of  
261 Mn<sub>3</sub>O<sub>4</sub>/graphene composites with great electrochemical properties for lithium-ion batteries. Rsc  
262 Adv. 2015;5:59208-59217.
- 263 28. Yue HW, Li F, Yang ZB, Li XW, Lin SM, He DY. Facile preparation of Mn<sub>3</sub>O<sub>4</sub>-coated carbon  
264 nanofibers on copper foam as a high-capacity and long-life anode for lithium-ion batteries. J Mater  
265 Chem A. 2014;2:17352-17358.
- 266 29. Luo S, Wu HC, Wu Y, Jiang KL, Wang JP, Fan SS. Mn<sub>3</sub>O<sub>4</sub> nanoparticles anchored on continuous  
267 carbon nanotube network as superior anodes for lithium ion batteries. J Power Sources,  
268 2014;249:463-469.
- 269 30. Park SK, Jin A, Yu SH, Ha J, Jang B, Bong S, Woo S, Sung YE, Piao Y. In situ hydrothermal  
270 synthesis of Mn<sub>3</sub>O<sub>4</sub> nanoparticles on nitrogen-doped graphene as high-performance anode  
271 materials for lithium ion batteries. Electrochim Acta, 2014;120:452-459.
- 272 31. Luo YQ, Fan SS, Hao NY, Zhong SL, Liu WC. An ultrasound-assisted approach to synthesize  
273 Mn<sub>3</sub>O<sub>4</sub>/RGO hybrids with high capability for lithium ion batteries. Dalton T. 2014;43:15317-15320.
- 274 32. Lavoie N, Malenfant PRL, Courtel FM, Abu-Lebdeh Y, Davidson IJ. High gravimetric capacity and  
275 long cycle life in Mn<sub>3</sub>O<sub>4</sub>/graphene platelet/LiCMC composite lithium-ion battery anodes. J Power  
276 Sources 2012;213:249-254.
- 277 33. Wang ZH, Yuan LX, Shao QG, Huang F, Huang YH. Mn<sub>3</sub>O<sub>4</sub> nanocrystals anchored on multi-  
278 walled carbon nanotubes as high-performance anode materials for lithium-ion batteries. Mater  
279 Lett. 2012;80:110-113.
- 280 34. Wang CB, Yin LW, Xiang D, Qi YX. Uniform carbon layer coated Mn<sub>3</sub>O<sub>4</sub> nanorod anodes with  
281 improved reversible capacity and cyclic stability for lithium ion batteries. ACS Appl Mater Inter.  
282 2012;4:1636-1642.
- 283 35. Li ZQ, Liu NN, Wang XK, Wang CB, Qi YX, Yin LW. Three-dimensional nanohybrids of  
284 Mn<sub>3</sub>O<sub>4</sub>/ordered mesoporous carbons for high performance anode materials for lithium-ion  
285 batteries. J Mater Chem. 2012;22:16640-16648.
- 286 36. Palaniandy N, Nkosi FP, Raju K, Ozoemena KI. Fluorinated Mn<sub>3</sub>O<sub>4</sub> nanospheres for lithium-ion  
287 batteries: Low-cost synthesis with enhanced capacity, cyclability and charge-transport. Mater  
288 Chem Phys. 2018;209:65-75.
- 289 37. Jiang Z, Huang KH, Yang D, Wang S, Zhong H, Jiang CW. Facile preparation of Mn<sub>3</sub>O<sub>4</sub> hollow  
290 microspheres via reduction of pentachloropyridine and their performance in lithium-ion batteries.  
291 RSC Adv. 2017;3:8264-8271.
- 292 38. Fan XY, Cui Y, Liu P, Gou L, Xu L, Li DL. Electrochemical construction of three-dimensional  
293 porous Mn<sub>3</sub>O<sub>4</sub> nanosheet arrays as an anode for the lithium ion battery. Phys Chem Chem Phys.  
294 2016;18:22224-22234.
- 295 39. Zhen MM, Zhang Z, Ren QT, Liu L. Room-temperature synthesis of ultrathin Mn<sub>3</sub>O<sub>4</sub> nanosheets  
296 as anode materials for lithium-ion batteries. Mater Lett. 2016;177:21-24.
- 297 40. Li TT, Guo CL, Sun B, Li T, Li YG, Hou LF, Wei YH. Well-shaped Mn<sub>3</sub>O<sub>4</sub> tetragonal bipyramids  
298 with good performance for lithium ion batteries. J Mater Chem A. 2015;3:7248-7254.
- 299 41. Bai ZC, Zhang XY, Zhang YW, Guo CL, Tang B. Facile synthesis of mesoporous Mn<sub>3</sub>O<sub>4</sub> nanorods  
300 as a promising anode material for high performance Lithium-ion batteries. J Mater Chem A.  
301 2014;2:16755-16760.
- 302 42. Huang SZ, Jin J, Cai Y, Li Y, Tan HY, Wang HE, Tendeloo GV, Su BL. Engineering single  
303 crystalline Mn<sub>3</sub>O<sub>4</sub> nano-octahedra with exposed highly active {011} facets for high performance  
304 lithium ion batteries. Nanoscale, 2014;6 : 6819-6827.



- 305 43. Jian GQ, Xu YH, Lai LC, Wang CS, Zachariah MR.  $\text{Mn}_3\text{O}_4$  hollow spheres for lithium-ion  
306 batteries with high rate and capacity. *J Mater Chem A*. 2014;2:4627-4632.
- 307 44. Zhao DY, Hao Q, Xu CX, Facile fabrication of composited  $\text{Mn}_3\text{O}_4/\text{Fe}_3\text{O}_4$  nanoflowers with high  
308 electrochemical performance as anode material for lithium ion batteries. *Electrochim Acta*,  
309 2015;180:493-500.
- 310 45. Wang JZ, Du N, Wu H, Zhang H, Yu JX, Yang DR, Order-aligned  $\text{Mn}_3\text{O}_4$  nanostructures as super  
311 high-rate electrodes for rechargeable lithium-ion batteries. *J. Power Sources*, 2013;222:32-37.
- 312 46. Wang M, Cheng LM, Li QB, Chen ZW, Wang SL. Two-dimensional nanosheets associated with  
313 one-dimensional single-crystalline nanorods self-assembled into three-dimensional flower-like  
314  $\text{Mn}_3\text{O}_4$  hierarchical architectures. *Phys Chem Chem Phys*. 2014;39:21742-21746.
- 315 47. Pasero D, Reeves N, West AR, Co-doped  $\text{Mn}_3\text{O}_4$ : a possible anode material for lithium batteries.  
316 *J Power Sources*. 2005;141:156-158.
- 317 48. Wang HL, Cui LF, Yang Y, Casalongue HS, Robinson JT, Liang YY, Cui Y, Dai HJ.  $\text{Mn}_3\text{O}_4$ -  
318 graphene hybrid as a high-capacity anode material for lithium ion batteries. *J Am Chem Soc*.  
319 2010;132:13978-13980.
- 320 49. Wu Z, Ren W, Wen L, Gao L, Zhao J, Chen Z, Zhou G, Li F, Cheng H. Graphene anchored with  
321  $\text{Co}_3\text{O}_4$  nanoparticles as anode of lithium ion batteries with enhanced reversible capacity and  
322 cyclic performance. *ACS Nano*, 2010;4:3187-3194.
- 323 50. Fei HL, Wei MD. Facile synthesis of hierarchical nanostructured rutile titania for lithium-ion battery.  
324 *Electrochim Acta*, 2011;56:6997-7004.
- 325 51. Fei HL, Li H, Li ZW, Feng WJ, Liu X, Wei MD. Facile synthesis of graphite nitrate-like ammonium  
326 vanadium bronzes and their graphene composites for sodium-ion battery cathodes. *Dalton Trans*,  
327 2014; 43:16522-16527.